Vertical land motion in the Southwest and Central Pacific from available GNSS solutions and implications for relative sea levels

Valérie Ballu, Médéric Gravelle, Guy Woppelmann, Olivier de Viron, Paul Rebischung, Melanie Becker, Pierre Sakic

Geophysical Journal International

Geophys. J. Int. (2019) **218,** 1537–1551
Advance Access publication 2019 May 27
GJI Gravity, Geodesy and Tides

doi: 10.1093/gji/ggz247

Vertical land motion in the Southwest and Central Pacific from available GNSS solutions and implications for relative sea levels

Valérie Ballu,[1] Médéric Gravelle,[1] Guy Wöppelmann,[1] Olivier de Viron,[1] Paul Rebischung,[2] Mélanie Becker[1] and Pierre Sakic[1,3]

[1] *LIENSs, Université de La Rochelle - CNRS,* 2 *rue Olympe de Gouges,* 17000 *La Rochelle, France. E-mail: valerie.ballu@univ-lr.fr*
[2] *IGN LAREG, Univ Paris Diderot, Sorbonne Paris Cité,* 5 *rue Thomas Mann,* 75205 *Paris Cedex* 13, *France*
[3] *Now at GFZ German Research Centre for Geosciences, Helmholtz Centre Potsdam, Telegrafenberg,* 14473 *Potsdam, Germany*

Accepted 2019 May 25. Received 2019 May 24; in original form 2018 December 19

SUMMARY

Coastal populations are impacted by relative sea level variations, which consist both of absolute sea level variations and of vertical land motions. This paper focuses on the Southwest and Central Pacific region, a recognized vulnerable region to sea level rise and where a large range of vertical land motion dynamics is observed. We analyse vertical displacement rates obtained from Global Navigation Satellite Systems (GNSS) by different analysis centres. We study the role played by modelled parameters, such as step discontinuities (due to equipment changes, earthquakes, etc.), in the position time-series analysis. We propose a new modelling approach based on a joint inversion of GNSS position time-series from different analysis centres. The final uncertainty on the vertical land motion rates is estimated as a combination of the uncertainty due to the GNSS data processing itself and the uncertainty due to the stability of the reference frame in which the GNSS data are expressed. We find that the dominant trend in the Southwest and Central Pacific is a moderate subsidence, with an average rate of -1.1 mm yr^{-1}, but significant variations are observed, with displacement rates varying from an uplift of 1.6 ± 0.3 mm yr^{-1} to a subsidence of -5.4 ± 0.3 mm yr^{-1}. Taking into account the geodynamic context, we assess, for each station, the relevance of current estimates of linear vertical displacement rate and uncertainty for forecasting future coastal sea levels.

Key words: Global change from geodesy; Satellite geodesy; Sea level change; Seismic cycle; Pacific Ocean; Time-series analysis.

1 INTRODUCTION AND BACKGROUND

When predicting the amount and effects of sea level change on coastal regions and developing adaption strategies to this change, the most relevant quantity is the sea level relative to the land. Relative sea level changes result from a combination of physical processes (from ocean, ice, atmosphere and solid Earth) acting over different spatial and timescales (Stammer *et al.* 2013). Vertical land motions and their estimates based on Global Navigation Satellite Systems (GNSS) measurements, in particular the Global Positioning System (GPS), have become an essential component in the relative sea level budget (Wöppelmann *et al.* 2007; Wöppelmann & Marcos 2016, for a review). Fig. 1 illustrates the relative importance of the ocean and solid Earth contributions to relative sea level change in the Southwest and Central Pacific region (45S/10 N and 145E/120 W). The values used in Fig. 1 come from research groups considered among the best in their field; these values vary between groups, but Fig. 1 indicates the order of magnitude of these processes.

Anticipating future relative sea level requires an understanding of the different factors contributing to its variations and their variability through time, with each factor having its own dynamics. Whether relative sea level is measured by tide gauges or derived from the combination of geocentric sea level (from satellite altimetry) and land motion (from space geodesy), evaluating and understanding current land motion, with associated uncertainty, is a key component in the forecasting of future relative sea levels.

This study focuses on this solid Earth contribution to relative sea level, for which scientists benefit from multiple estimates provided by various internationally acknowledged space geodesy groups. The process of estimating vertical land motion rates from GNSS measurements is not straightforward, involving several steps such as computing daily positions from GNSS measurements (in which many other parameters such as orbits, clocks and atmospheric delays are also adjusted), referencing these positions in a stable geocentric reference frame and modelling and inverting the position time-series to obtain the quantity of interest (trends, cycles, step discontinuities,

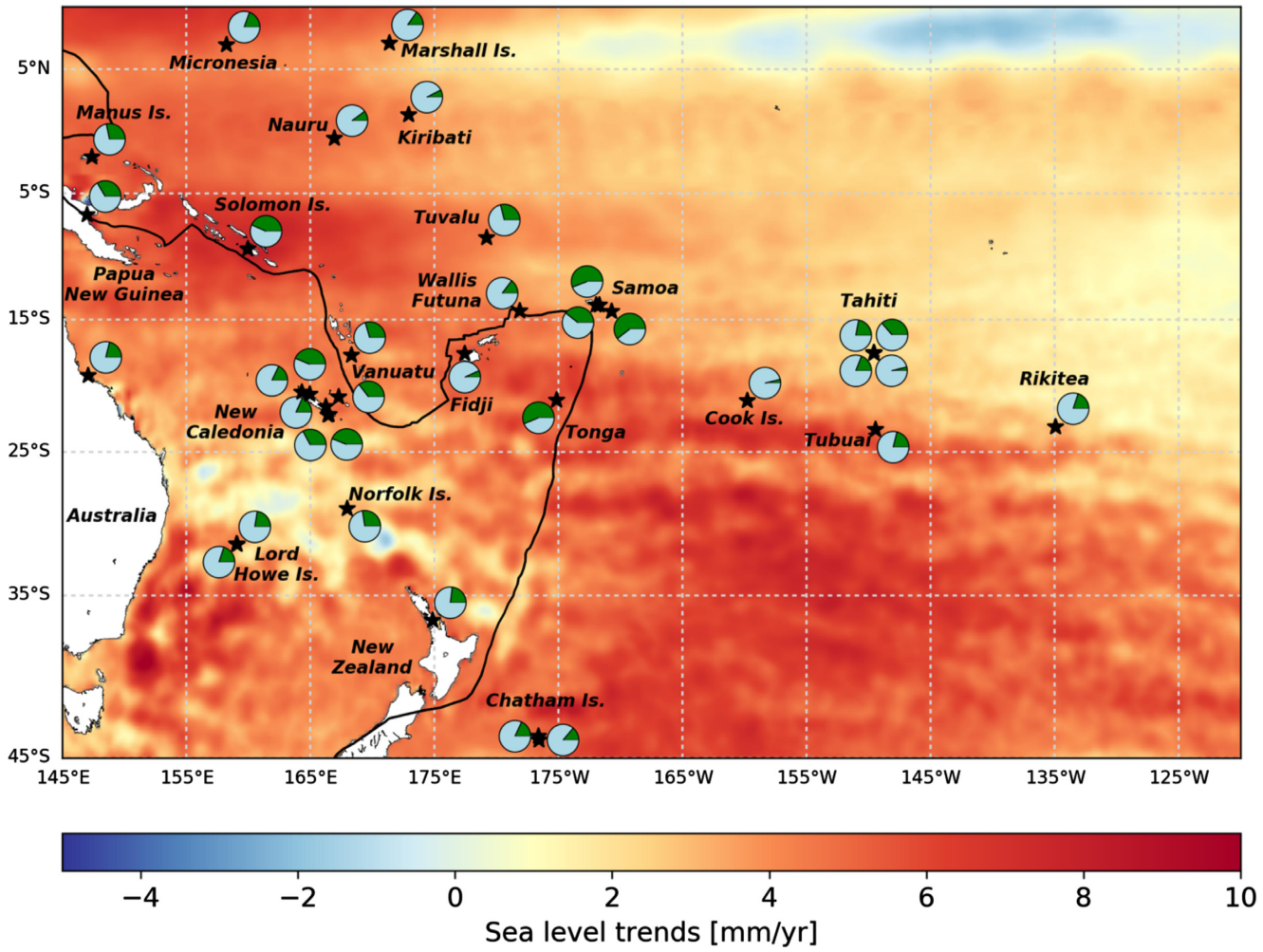

Figure 1. Study location map. The background map shows the temporal evolution of the global Mean Sea Level (MSL) (DOI: 10.5270/esa-sea_level_cci-IND_MSL_MERGED-1993_2015-v_2.0–201 612 and Ablain *et al.* 2015), provided by European Space Agency in the framework of the Climate Change Initiative (ESA CCI). It illustrates the magnitude and spatial variability of sea level trends (1993–2015) in the area of study. Pie charts, at each GNSS station emplacement, show respective order of magnitude of absolute sea level variations (light blue) and vertical land motion (green). In this example, the land motion value is the absolute value of the trend obtained using Midas by NGL (available for every station) and the sea level trend is interpolated at the station location from the ESA CCI sea level trend (described above). The black line corresponds to the tectonic plate limit between the Indo-Australian Plate and the Pacific Plate, as proposed in the Morvel-25 plate boundary model (DeMets *et al.* 2010).

etc.). Each of these steps involves analyst choices which can significantly affect the estimated values of the quantity of interest, for example the value of a linear trend—representing a steady land motion—versus the amplitude of step discontinuities representing sudden displacements due, for instance, to earthquakes (coseismic displacements). When the estimates provided by different analysis centres agree within their error bars, they raise confidence and allow geophysical interpretation. However, differences between estimates can be statistically significant, even for GNSS solutions produced by the groups participating in the International GNSS Service (IGS, Dow *et al.* 2009) and contributing to the realization of the International Terrestrial Reference Frame (ITRF, Altamimi *et al.* 2017).

Evaluating vertical land motion in the Southwest and Central Pacific (Fig. 1) is of special interest for several reasons:

(i) The rate of sea level rise in the Southwest Pacific region is higher than the globally averaged rate, and is spatially variable within the region (Becker *et al.* 2012; Martínez-asensio *et al.* 2019),

(ii) There are many low-elevation islands, whose inhabitants are particularly vulnerable to sea level rise. Appropriate adaptation strategies are needed and require a precise evaluation of the contribution of vertical land motion to relative sea level (Nurse *et al.* 2014),

(iii) The number and distribution of GNSS stations in the region is limited and the complex tectonic setting means that vertical land motions can be significantly different from place to place (see Section 2),

(iv) Only a few sites are continuously monitored within the region and the relative weight of these sites in global studies is therefore higher than those in regions with dense GNSS station coverage. These global studies—such as ITRF realization, the detection of satellite altimetry drift, and past sea level reconstructions—may have consequences at different spatial scales, including local sea level studies.

Fig. 2 shows examples of available vertical position time-series and rate estimates for the GNSS stations of KIRI and NRMD (IGS acronyms), located in Tarawa, Kiribati and Nouméa, New-Caledonia, respectively. Although the vertical rates of land motion are relatively small at these sites, accurate rate estimates are needed.

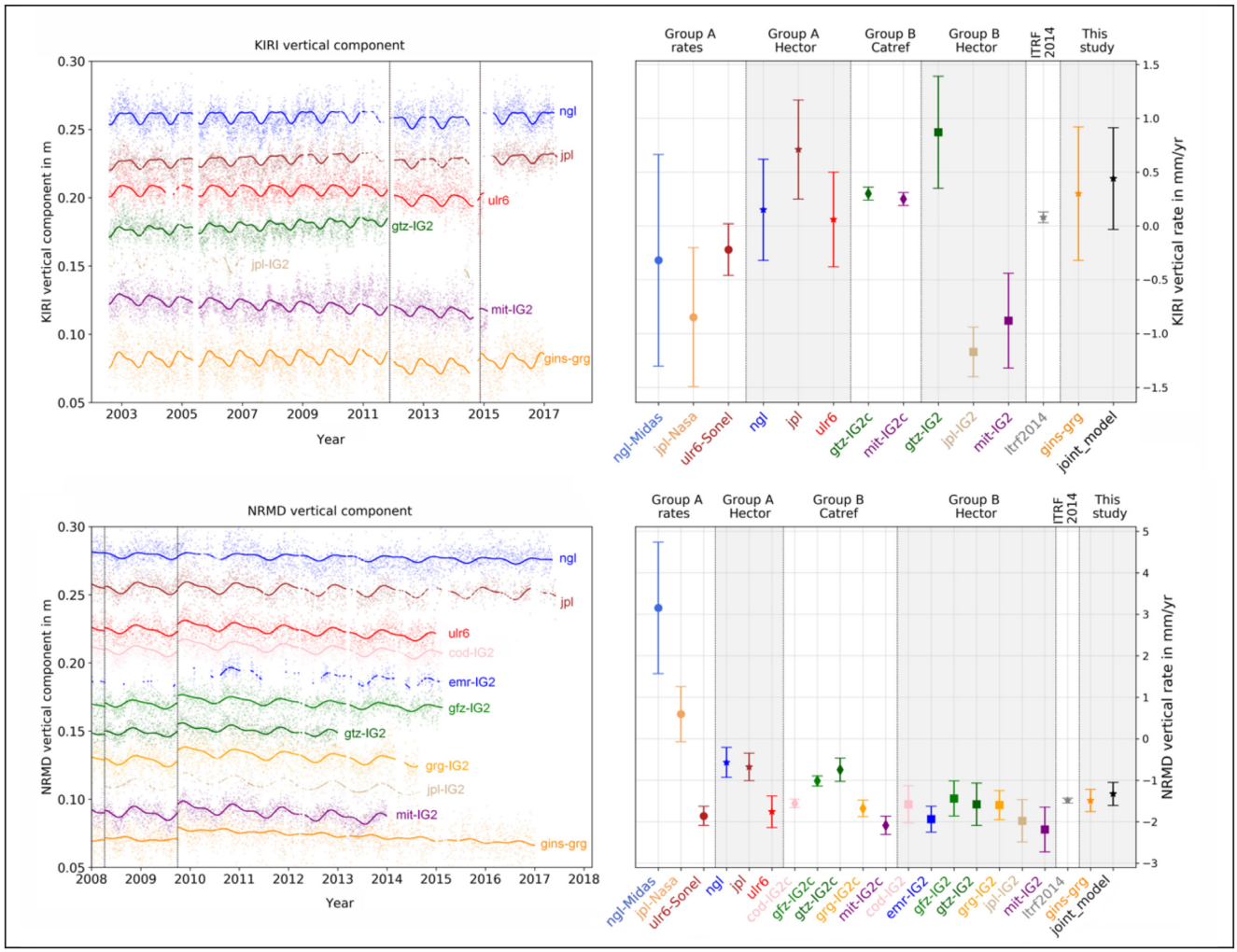

Figure 2. GPS position time-series and vertical velocity estimates for Kiribati GPS station (KIRI, upper panels) and Nouméa GPS station (NRMD, lower panels). The left-hand panels show the vertical position time-series as provided by different analysis centres, easily available to the users (Group A), provided to the IGS (Rebischung *et al.* 2016) as their contribution to the reprocessing campaign IGS REPRO2 (Group B), or computed as part of this study using GINS software (Marty *et al.* 2011, gins-grg solution). The time-series data are shown as pale colour and the model fit for each solution is superimposed in stronger colour. Vertical black lines indicate the step discontinuities used in our study (see Table S4). The right-hand panels display the vertical rates and associated uncertainties modelled using various methods. The information on the data sources, processing methods and labels is given in Tables 1a and b, and further detailed in Section 3.

In Kiribati, the need is associated with the high societal impact of sea level rise (Wyett 2014). In Nouméa, the need is associated with the availability of a long tide-gauge record, for which any error in the local GNSS rate estimate impacts the reconstruction of past global mean sea levels and the calibration of satellite altimeters (Aucan *et al.* 2017). Fig. 2 also illustrates the following issues:

(1) Some analysis centres do not include all stations, and thus do not necessarily provide a solution for every station of interest.

(2) Some solutions do not include all the observations available at a given station.

(3) Different rate estimates can be obtained from the same observations, depending on the data analysis strategy (modelling, adjustment strategy, etc.).

(4) Uncertainty estimates can differ greatly from one solution to the other.

(5) Differences between the rate estimates can be larger than the error bars provided by the analysis centres.

Part of the differences illustrated in Fig. 2 arises from different choices in GNSS data analysis strategies, even though the highest international standards were adopted (Petit & Luzum 2010) in all solutions presented here. Comparison experiments of GNSS products are organized at regular intervals within IGS to assess the performance of cutting-edge data analysis strategies (Collilieux *et al.* 2011, Rebischung *et al.* 2016), but these comparisons are carried out on a global scale that can hide regional issues. For instance, the alignment to the reference frame and its errors is known to map differently depending on the region considered (Collilieux & Wöppelmann 2011), meaning that errors due to referencing issues that are minimized at the global scale, may be more significant at the regional scale. In a case study on Europe, Legrand *et al.* (2010) showed systematic errors of several millimetres per year in regional networks of stations, especially for the vertical component of the station position and velocity estimates (up to 2.9 mm yr^{-1} difference). In addition to the geographic extent of the network of stations, the use of a consistent GNSS data analysis strategy across the data time span has also proven to be a key factor in obtaining

consistent results, especially in the vertical component (Steigenberger *et al.* 2006; Wöppelmann *et al.* 2007; Collilieux *et al.* 2011). Since we are aiming for better than 1-mm yr^{-1} accuracy on ground displacement signals, the highest precision of GNSS positioning is required; hence we only consider global and reprocessed solutions in this study.

Once the first step of obtaining global reprocessed GNSS solutions (daily positions) is properly achieved, the second step (hereafter called 'step 2″) of estimating vertical land motion rates and uncertainty from the position time-series also impacts the final results. Most analysis centres provide the position time-series as well as a linear trend, even though the motion may be more complicated than a linear trend.

A well-known issue associated with the GNSS position time-series is the presence of step discontinuities (Griffiths & Ray 2016), either caused by equipment changes (e.g. antenna, receiver, cable, firmware), environmental changes (e.g. trees, buildings) or geophysical phenomena (e.g. coseismic displacement due to an earthquake). Many discontinuity epochs are known from station site logs (metadata) or from earthquake inventories, but some remain undocumented. Their presence impacts vertical land motion rate estimates (Williams 2003), but to date there is no entirely satisfying automatic solution to cope with this issue. Blind tests conducted during the DOGEx experimentation (Gazeaux *et al.* 2013) on the detection of step discontinuities in GPS position time-series concluded that the human eye performs better than any automatic methods yet developed. Consequently, different sets of step discontinuities are identified and adopted by analysis centres from different expert eyeball or automatic procedures, ultimately leading to differences in velocity estimates.

In this study, for each station of interest, we first provide a homogeneously reprocessed time-series of daily positions computed using the GINS software (developed by CNES/GRGS, Marty *et al.* 2011) with GRG orbit and clock products (Section 3.1.2). Then, using the position time-series provided by the various analysis centres, we perform the time-series analysis (step 2) using a common set of step discontinuities and a time-correlated noise model to derive a linear trend (velocity) and its associated uncertainty. We then compare our results for each station across the analysis centres and with the results given by each analysis centre. Finally, to address the question of which available GNSS solution could be used for geophysical interpretation and potential relative sea level studies, we propose a new methodology using all of the available position time-series in a joint inversion. The outcome is a new set of vertical land motion estimates and uncertainties for all the stations in our area of interest. We evaluate the ability of this new data set (velocity and uncertainty) to help in the forecasting future sea level changes and hazards.

2 SALIENT TECTONIC FEATURES OF THE SOUTHWEST AND CENTRAL PACIFIC ISLAND REGION

The objective of this section is to highlight salient tectonic features in the Southwest and Central Pacific region. This vast region (Fig. 1) encompasses active tectonic areas to the west and a quiet domain without seismic activity to the east and the north. Islands in the Southwest and Central Pacific on which the GNSS stations are installed are of different natures, with coral atolls and subduction arc islands as end-members. Two tectonic plates, the Indo-Australian and the Pacific ones, converge towards each other at a mean rate of about 10 cm yr^{-1}. This convergence is accommodated by two major subduction zones: the east-dipping New Hebrides/Salomon/Papua-New Guinea subduction zone, where the Australian Plate is subducting; and the west-dipping Tonga-Kermadec subduction zone, where the Pacific Plate is subducting. Between these two subduction zones lies a complex deforming domain around the Fiji islands with spreading and strike-slip features (e.g. Pelletier *et al* 1998).

The subsidence of Pacific volcanoes as they age was proposed by Darwin (1842) to explain the formation of low lying coral atolls generated from elevated volcanic structures. Although the integrated vertical motion over millions of years reaches kilometre scales, the displacement rates are very small, likely on the order of 0.1 mm yr^{-1}. For instance, Pirazzoli & Montaggioni (1985) estimate a subsidence rate of approximatively 0.05 mm yr^{-1} in the Leeward Islands of the Society archipelago. Post-glacial isostatic adjustment in the studied area contributes from −0.1 to −0.3 mm yr^{-1} of vertical motion, according to the ICE6G-VM5a model (Argus *et al.* 2014; Peltier *et al.* 2015). These non-tectonic contributions, together with the cooling of the lithosphere away from spreading ridges, can be assumed to be linear at the scale considered in our study and for century scale projections; their combined maximum amplitude should be less than 1 mm yr^{-1}.

In contrast, seismic cycle related processes are highly unsteady, with rapid and possibly centimetre- to metre-scale amplitude displacements related to strain accumulation and release in the vicinity of plate tectonic boundaries. Fig. 3 illustrates the maximum vertical displacement (absolute values) induced by earthquakes over the period 1975–2018; it is modelled from the Global Centroid-Moment-Tensor (CMT) earthquake catalog (www.globalcmt.org) using Okada (1985) equations (modelling information can be found in Métivier *et al.* 2014). Although 40 yr is short with respect to the length of seismic cycles (several decades, centuries or even millennia), this map highlights zones prone to earthquake-induced vertical land motion. Some of the studied stations such as VANU, SOLO and SAMO, located in the direct vicinity of a subduction zone, are expected to experience substantial vertical land motion. Others, for instance in the French Polynesia area or Kiribati region—hereafter named intraplate stations—are unlikely to be affected by earthquake. Finally, the remaining stations, such as NOUM, NRMD or AUCK, may be affected by tectonic motion, although neither strongly nor frequently.

3 MATERIAL AND METHODS

3.1 Description of data

In this study, the primary data sets are time-series of daily vertical positions computed from GNSS measurements. The second set of data are the rate estimates of vertical land motion obtained by the analysis centres themselves after step 2 of GNSS data analyses (Tables 1 and S1).

The length of the series is critical for accurate determination of vertical displacement rates, due to seasonal variations and correlated noise (e.g. Blewitt & Lavallée 2002). Here, we choose to retain only solutions covering a minimum of 7 continuous years, except for station TBTG in Tubuai which we kept, despite a nearly 2-yr gap around 2015, because of the small number of stations in the area. We limit our study to the period before 2017 because of the adoption of a new antenna model at the beginning of 2017 (related to the change from ITRF2008 to ITRF2014), implying the need for a change in the modelled parameters of the position time-series analysis.

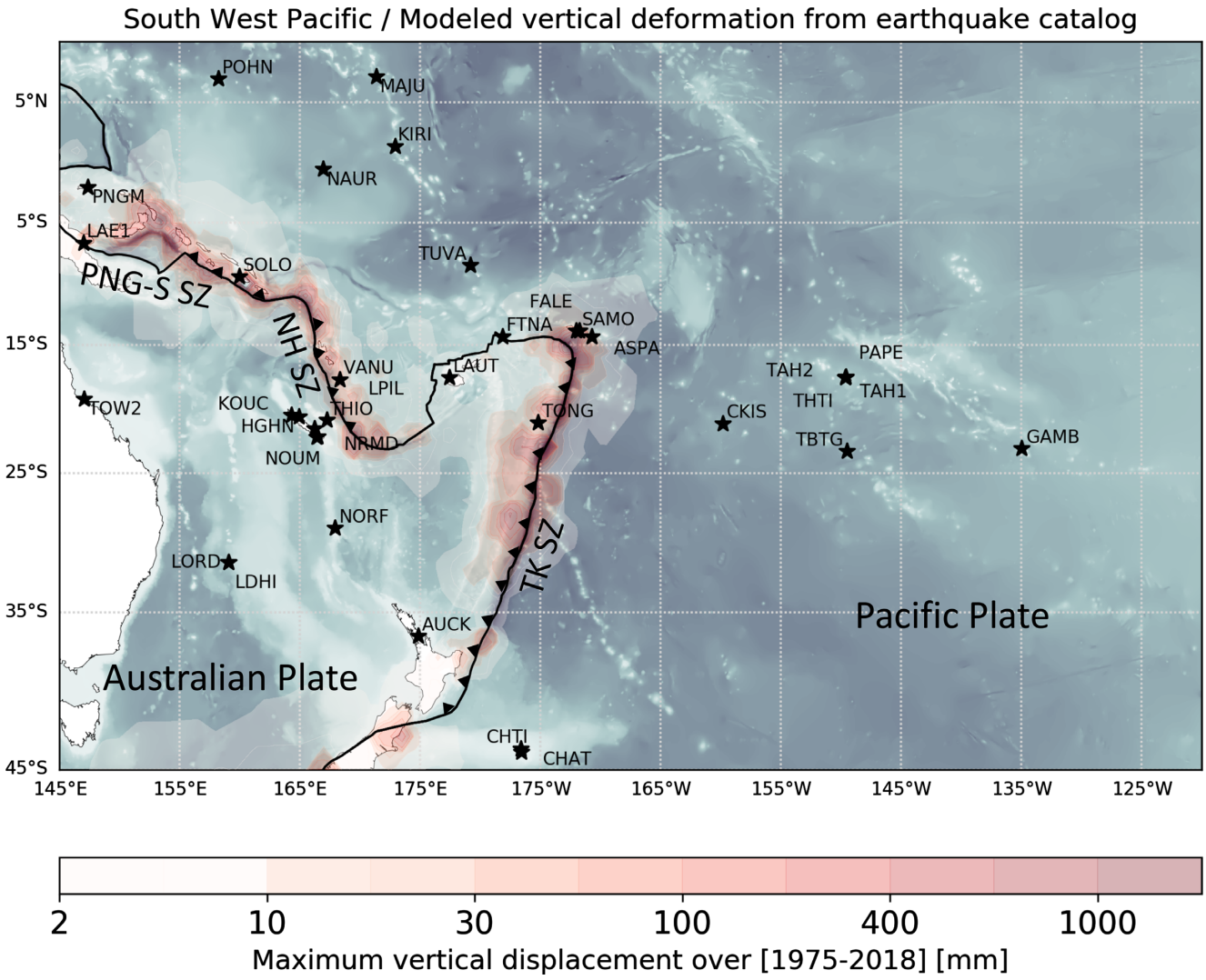

Figure 3. Map of the study area, indicating the stations (stars) with a long enough GPS record available (∼>7 yr, see Section 3). The background grey/blue shading highlights the bathymetric features in the oceanic domain, based on GEBCO_2014 (Weatherall *et al.* 2015) bathymetric data. The red shading indicates maximum absolute values of vertical displacement modelled using Okada (1985) dislocation model and the USGS earthquakes catalog (see Métivier *et al.* 2014 for a description of the computation method), for the period 1975–2018. The black line corresponds to the tectonic plate limit between the Australian Plate and the Pacific Plate, as proposed in the Morvel-25 plate boundary model (DeMets *et al.* 2010). The subduction zones are indicated by triangles on the over-riding plate, and labelled TK SZ, NH SZ and PNG-S SZ, respectively for the Tonga-Kermadec, New Hebrides and Papoua-New Guinea—Salomon subduction zones.

3.1.1 Available public GNSS solutions

We use only free, publicly available, GNSS solutions based on a global network of stations and a free-network approach (Heflin *et al.* 1992) or loosely constrained data analysis strategy (Altamimi *et al.* 2002) that is consistent across the data time span (reprocessing). In this study, the expression 'GNSS solutions' corresponds to the daily station position time-series obtained after the first step of the GNSS data analyses and/or estimates of displacement rates (linear trends) obtained after step 2.

We consider two categories of public GNSS solutions (Table 1):

1) Group A: widely used and publicly available solutions (daily position time-series and rates) provided by the Nevada Geodetic Laboratory (NGL, http://geodesy.unr.edu/ Blewitt *et al.* 2016), by the Jet Propulsion Laboratory (JPL) under contract with NASA (https://sideshow.jpl.nasa.gov/post/series.html, Heflin 2018), and by the University of La Rochelle (ULR) under the SONEL framework (http://www.sonel.org/, Santamaría-Gómez *et al.* 2017). Each of the three data sets comes with a table providing (linear) rate estimates and associated uncertainties for the horizontal and vertical positioning components (these products are denoted Group A/rates in Table 1b and Fig. 2). The NGL solution rates are estimated using the MIDAS (Median Interannual Difference Adjusted for Skewness) method, which is based on the median of slopes computed between pairs of data (Blewitt *et al.* 2016) and does not require the identification and determination of step discontinuities. In contrast, the JPL and ULR solutions are based on the least-squares adjustment of a model aimed at describing the time evolution of the station positions, which requires the identification of step discontinuities and their subsequent adjustment as parameters of the model (see, respectively Heflin 2018 and Santamaría-Gómez *et al.* 2017, for details). These three solutions are available for many stations not

Table 1. List of GNSS solutions and type of processing considered in our study. PPP (Precise Point Positioning) can be used to compute the position parameters of a single station using previously determined orbits and clock products, whereas Double Differences methods require the computation of position parameters for a network of stations. Table 1a lists the data sources and Table 1b gives the link between the data source, the type of processing and the labels of the results as used in Fig. 2. In Table 1b, single position time-series refers to the processing of each time-series individually for each analysis centre.

Table 1a

	Solution/acronym	Analysis Centre/Reference	Method (Software)	GNSS data
Group A	ngl	Nevada Geodetic Laboratory *http://geodesy.unr.edu/*, Blewitt *et al.* 2016 velocity file: *http://geodesy.unr.edu/velocities/midas.IGS08.txt*	PPP (Gipsy-Oasis)	GPS
	jpl	Jet Propulsion Laboratory *https://sideshow.jpl.nasa.gov/post/series.html* velocity file: *https://sideshow.jpl.nasa.gov/post/tables/table1.html*	PPP (Gipsy-Oasis)	GPS
	ulr6	University of La Rochelle *http://www.sonel.org/*, Santamaría-Gómez *et al.* 2017 velocity file: *http://www.sonel.org/IMG/txt/vertical_velocities_table.txt*	Double Differences (GAMIT/Globk, CATREF)	GPS
Group B	cod-IG2	Centre for Orbit Determination in Europe	Double Differences (Bernese)	GPS/GLONASS since 2002
	emr-IG2	Natural Resources Canada	Zero differences (Gipsy-Oasis)	GPS
	esa-IG2	EuropeanSpace Operations Centre	Zero differences (NAPEOS)	GPS/GLONASS since 2009
	gfz-IG2	GeoForschungsZentrum	Zero differences (EPOS)	GPS
	gtz-IG2	GeoForschungsZentrum	Zero differences (EPOS)	GPS
	grg-IG2	Groupe de Recherche en Géodésie Spatiale	Zero differences (GINS)	GPS/GLONASS since 2009
	jpl-IG2	Jet Propulsion Laboratory	Zero differences (Gipsy-Oasis)	GPS
	mit-IG2	Massachusetts Institute of Technology	Double Differences (GAMIT/Globk)	GPS

Table 1b

	Data	**Processing**	**Label**
Group A	vertical rates	performed by the analysis centres	Group A/rates
	single position time-series	Hector	Group A/Hector
Group B	single position time-series	Catref	Group B/Catref
	single position time-series	Hector	Group B/Hector
ITRF2014	vertical rates	performed by IGS	itrf2014
This study	single position time-series	Hector	gins-grg
	all position time-series	joint least-squares modelling	joint_model

included in the ITRF realizations and can be downloaded by non-GNSS specialists. These users will hopefully find here interesting comparisons and an independent assessment of the reliability and accuracy of the position time-series, vertical displacement rates and uncertainties derived from our analysis of these solutions. Rates and uncertainty estimates are reported for all the available stations in the area in the Supplementary Material (Table S1).

2) Group B: the position time-series provided to the IGS by eight analysis centres as their contribution to the second GNSS reprocessing campaign (hereafter called REPRO2 and labelled IG2) and the last realization of the ITRF (ITRF2014, Rebischung *et al.* 2016). Note that since we use the ULR6 solution, updated with data from year 2014, in Group A, we do not use the ulr-IG2 time-series. For the Group B solutions, we first obtained the vertical displacement rates by stacking the daily REPRO2 solutions of each analysis centre (Rebischung *et al.* 2015) using CATREF software (Altamimi *et al.* 2007); these rates are labelled 'Group B/Catref' and '-IG2c' in Table 1b and Fig. 2.

All daily position time-series considered here for Group A and Group B are expressed in the ITRF2008 frame. The transformation parameters between ITRF2008 and ITRF2014 (http://itrf.ign.fr/ITRF_solutions/2014/tp_14-08.php) are small in terms of rates: in our region of interest, the impact is about 0.2 mm yr^{-1} on the station vertical velocities, hence relatively negligible compared to the large differences observed from one solution to the other (Fig. 2 for KIRI and NOUM and Supporting Information—Fig. S2 and Table S1—for all other stations).

3.1.2 Our dedicated GNSS solution using the GINS software

To allow a relevant comparison, each station of interest should appear in at least two solutions over the 1996–2016 period of available

GNSS observations. The NGL solution contains all the stations, but a number of stations (e.g. HGHN, THIO, FALE, GAMB, LDHI) are not computed by the other centres. Merging results from different GNSS solutions can lead to inconsistencies and errors, especially when studying relative displacements between stations (spatially correlated processing and referencing errors may not cancel out in the differences between stations). This is why we computed our own daily position time-series from the GNSS measurements for all the stations in the study area. We used the processing software GINS developed at CNES/GRGS (Marty *et al.* 2011) to compute our solution using processing features described in Table 2; GINS software is used for a growing number of high-precision positioning applications such as the Precise Point Positioning (PPP) of buoys in kinematic mode (Fund *et al.* 2013), but has not yet been widely used to quantify slow ground displacement over long timescales. GINS software has also been used by one of the operational IGS analysis centres for a decade or so. We also use the GINS software due to its fast computation speed (PPP rather than double-differences) and flexibility. A side outcome of this exercise is to assess the relevance of using the GINS software in PPP mode for precise tectonic studies or sea level related studies at the local/regional scales as an easily implemented alternative to other widely used software packages (GAMIT, GIPSY, BERNESE, etc.).

3.2 Overall time-series analysis of daily position time-series

3.2.1 Available time-series reanalysis using a common tool and model

One of the widely used outputs of vertical position time-series analysis are linear trends (rates) of vertical displacement (when appropriate). These linear trends are one of the components of the functional or trajectory model (Bevis & Brown 2014) used for the GNSS data analysis step 2. This functional model generally includes a periodic signal (annual and semi-annual), a linear trend, step discontinuities and, in some cases, logarithmic/exponential signals due to post-seismic deformation. We have used such a functional model in our analysis and the vertical ground motion $z_k(t)$ observed by the GNSS solution k can be written in the following form (eq. 1):

$$z_k(t) = \alpha_k + \beta_k t + \sum_{i=1}^{N_{jumps}} \gamma_{k,i} H(t - t_i) + \sum_{j=1}^{N_{log}} \delta_{k,j} \log\left[1 + H(t - t_j)\frac{(t - t_j)}{\tau l_j}\right] + \sum_{p=1}^{N_{exp}} \epsilon_{k,p} H(t - t_p)\left(1 - e^{-\frac{(t-t_p)}{\tau_{ep}}}\right) + \zeta_k \cos\left(\frac{2\pi t}{T}\right) + \eta_k \sin\left(\frac{2\pi t}{T}\right) + \chi_k \cos\left(\frac{4\pi t}{T}\right) + \psi_k \sin\left(\frac{4\pi t}{T}\right), \quad (1)$$

where

(1) $H(t - t_i)$ is the Heaviside Function, which is equal to zero for a negative argument and one for a positive argument, t_i being the discontinuity epochs (the list of discontinuity epochs is given in Table 4 and Table S4).

(2) α_k and β_k are the coefficients of a degree one polynomial to model the linear trend,

(3) $\gamma_{k,i}$ corresponds to the amplitude of the ith step discontinuity occurring at epoch t_i,

(4) $\delta_{k,j}$ corresponds to the amplitude of the jth logarithmic decay of relaxation time τ_{lj} occurring at epoch t_j.

(5) $\epsilon_{k,p}$ corresponds to the amplitude of the pth exponential decay of relaxation time τ_{ep} occurring at epoch t_p.

(6) ζ_k and η_k are the amplitude coefficients of the annual signal and χ_k and ψ_k are the amplitude coefficients of the semi-annual signal, T being the 1-yr period.

At this stage, we assume that, for each station, the parameters β, γ, δ, and ε (eq. 1) are the same for all time-series at that station, along with the number and time of the jumps and the postseismic signals (if included).

Vertical displacement rates (β in eq. 1) and their associated uncertainties are usually provided by analysis centres (see Section 3.1 and Table S1), but these rates and uncertainties are highly dependent on the epoch and the amplitude of step discontinuities (Williams 2003; Griffiths & Ray 2016) and are sensitive to modelling details, notably the accounting for time-correlated noise. Previous studies have demonstrated that modelling noise in continuous GNSS time-series from global solutions as white noise plus flicker noise generally provides more realistic uncertainties than assuming only white noise (Williams *et al.* 2004; Santamaría-Gómez *et al.* 2011; Wang *et al.* 2012). For instance, Mao *et al.* (1999) showed that uncertainty may be underestimated by a factor 5–11 when a pure white noise model is assumed and Langbein (2012) showed that using a flicker or flicker plus random walk for the time-dependent noise model changes the final uncertainty by a factor of two. Although difficult to assess without long records, a low amplitude random-walk noise can also impact velocity estimates and uncertainty (Williams *et al.* 2004; Langbein 2012).

Therefore, a direct comparison of rates and uncertainties provided by the analysis centres using different step discontinuities and modelling choices cannot be rigorous. This argues in favour of re-analysing the available GNSS position time-series using one model and methodology, so that consistent products and error bars can be compared; here we chose to use the functional model described in eq. (1), the Hector software package (Bos *et al.* 2013) and a common set of discontinuity epochs for all the time-series available for each station (the discontinuity table is given in Table S4). Like the CATS software (Williams 2008), the Hector software uses the Maximum Likelihood Estimation (MLE) method and can account for a large variety of temporal correlated noise. For our study, which focuses on the vertical component, we did not re-investigate the noise modelling issue and we use the Hector software with a white plus flicker noise model to derive linear trends of vertical displacements and associated uncertainties. In addition to the modelling of a linear trend and step discontinuities at known epochs, the Hector software allows the removal of outliers prior to modelling, the modelling of periodic signals of known periods and the modelling of post-seismic deformation if needed (discussed below).

Stations displacement rates and uncertainties obtained using a homogeneous analysis based on the Hector software and identical discontinuity epochs are displayed in Fig. 2 (right-hand panel) and in Table S1 of the Supporting Information to allow the comparison with rates and uncertainties provided by the analysis centres or obtained by stacking the daily REPRO2 solutions of each IGS analysis centre using the CATREF software (Altamimi *et al.* 2007; Rebischung *et al.* 2015). The link between labels in Fig. 2 and the data source/processing method is given in Table 1b.

The direct correlation between the estimated step discontinuity and linear trend of a time-series must be kept in mind when analysing results; although its impact varies with the position of the step in

Table 2. Main processing features of our proposed GPS solution using the GINS software.

Parameter	Description
GPS software	GINS
Method	IPPP (Precise Point Positioning with Integer ambiguity fixing)
Sessions and sampling	24 hr, decimated at 5 min
Elevation cut-off	10°
Troposphere refraction	GPT2 (Lagler *et al.* 2013)
Antenna PCV	IGS08 week 1935 (igs08.atx)
Earth orientation	IERS Bulletin B, Non-Rotating Origin
Earth and polar tide	IERS 2003 conventions
Ocean tide loading	FES2004
Orbit/clock products	GRG2 (GRG orbits/clocks reprocessed in the framework of IGS-REPRO2 campaign when available), operational GRG products otherwise.
Reference frame	ITRF2008

the time-series. In our data set, three time-series, CHAT, CHTI and NORF, have a single discontinuity epoch (see Supporting Information) and can be used to quantify the correlation coefficients, which are respectively 0.84, 0.81 and 0.74 for these series. This correlation and the impact of the choice of discontinuity epochs on the estimated trend is illustrated on Fig. 4 for the station PNGM.

The impact on the linear trend estimates of the correlation between the discontinuity amplitude and the linear trend is illustrated in Fig. 5, where discontinuity amplitudes are modelled jointly across the solutions (see Section 3.2.2) or independently for each solution, using identical discontinuity epochs.

3.2.2 Joint least-square modelling

The last step of our approach is to try to provide the user with an estimate for a linear vertical displacement rate, when appropriate, as well as a reasonable uncertainty estimate to be used for further interpretation. As mentioned earlier, numerous high-quality GNSS solutions are available for users, with no obvious criteria for selecting between them; the question here is how one can deal with these solutions in practice, for instance for sea level variation studies. A weighted mean or median of the solutions are standard metrics used to obtain a single estimate for each station. These two metrics agree in general; however, a disagreement between them highlights an asymmetry in the data distribution that should be further investigated. In addition, the fact that we may be estimating strongly correlated parameters using noisy data may lead to ill-resolved individual parameters. We propose to take advantage of the fact that different solutions may be affected by noise in a different way, and perform a joint least-squares inversion (modelling) based on all the available time-series.

Since the slope estimate and the amplitude of step discontinuities in the time-series are not well separated in the least-squares fit, imposing the same discontinuity amplitude for the time-series from different analysis centres ensures that the slope is modelled with the same hypothesis for each analysis centre.

Modelling a common amplitude for step discontinuities is definitely appropriate when the origin of the offsets is documented as ground motion such as an earthquake or a clear vertical shift induced by an antenna height change. However, such common modelling is more subjective if the step discontinuity is of unknown origin or whose origin may be considered differently by different processing methods, such as a change in receiver firmware.

In our data set, four stations show substantial post-seismic deformation (Fig. S2): ASPA, FALE and SAMO (in the American Samoa and Samoa). They were affected by the M8.1 Samoa earthquake in 2009, and VANU in Port-Vila, Vanuatu, was affected by a *M*7.3 earthquake in 2010. Following the example given in the Hector user's manual, we use constant relaxation times of, respectively, 10 and 100 d for the logarithm and exponential decay components; these values provide an adequate model fit for individual position time-series modelling with Hector (Section 3.2.1, Fig. S2 in the Supporting Information) for the four stations and are kept in the least-squares joint inversion.

The terms of geophysical origin, such as the slope (β_k) and the earthquake-related terms should be common to all series, but this is less clear for signatures related to equipment changes. Annual and semi-annual signals may include site specific geophysical effects, but also GNSS processing dependent parameters (from step 1), thus we decided not to fit common annual and semi-annual signals. After testing different configurations, we chose to retain the following configuration for our joint inversion: (1) all the parameters, except for $\alpha_k$and the annual/semi-annual parameters (ζ_k, η_k, χ_k and ψ_k), are considered to be the same for all the solutions, and therefore only one estimate based on all the time-series, is obtained for these parameters: the amplitude of step discontinuities, the slopes and post-seismic deformation parameters (logarithm and exponential coefficients and relaxation time). This can be written as:

$$\beta_k = \beta, \quad \gamma_{k,i} = \gamma_i \ , \quad \delta_{k,j} = \delta_j \ , \quad \epsilon_{k,p} = \epsilon_p \ , \ \forall k \tag{2}$$

The estimates of the parameters associated with the joint model are given in the Supporting Information (Table S5) for all the stations.

3.2.3 Rate displacement uncertainties

The estimation of the uncertainties on GNSS vertical velocities or rate displacements is not straightforward. Two distinct contributions can be taken into account: the uncertainty of the velocity within a specific reference frame (here ITRF2008) and the uncertainty due to the reference frame itself.

We start by the estimation of the uncertainty in the determination of the velocities within the ITRF2008, in which all the GNSS data processing was performed. The formal error from the least-squares fit is known to be underestimated due to time-correlated noise (Santamaría-Gómez *et al.* 2011) and to the fact that the position time-series from different groups are based on the same data. Note that the configuration—the large number of data points and the correlation between signals—makes a bootstrap method inefficient unless we first arbitrarily decimate the data to account for the degree

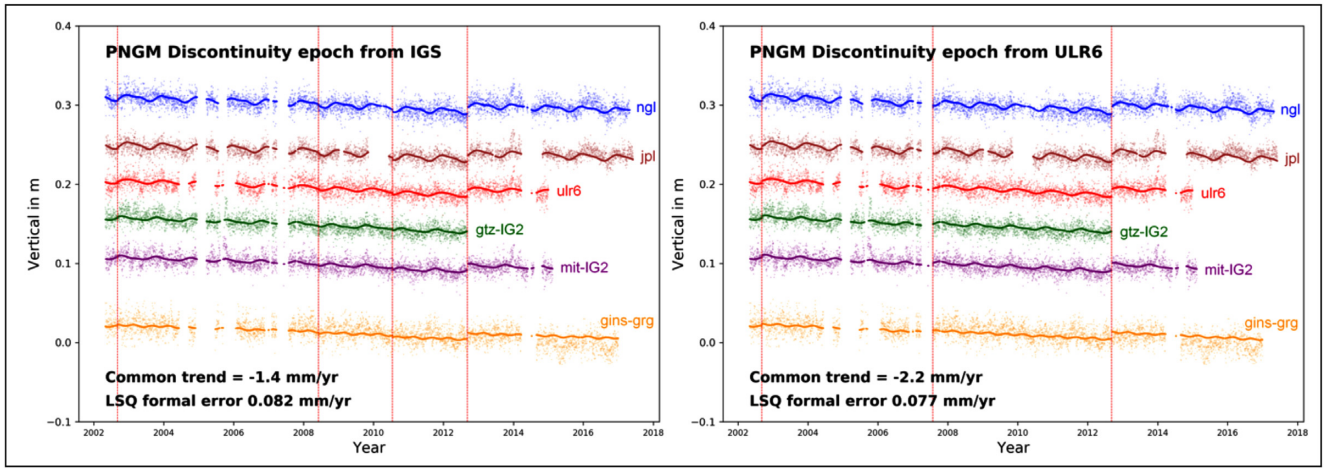

Figure 4. Illustration of the effect of choosing different discontinuities epochs. The time-series data are shown as pale colour and the model fit for each solution is superimposed in stronger colour. In the left-hand panel, the discontinuity epochs are taken from the IGS discontinuity file used for ITRF2014 realization, whereas in the right panel, the discontinuity epochs are taken from the Sonel/ULR6 discontinuity file. This figure illustrates the correlation between slopes and discontinuity epoch. Note that in this example, in order to reduce the sensitivity to a single time-series noise and increase the robustness of the fit, a common offset amplitude has been adjusted on all the time-series.

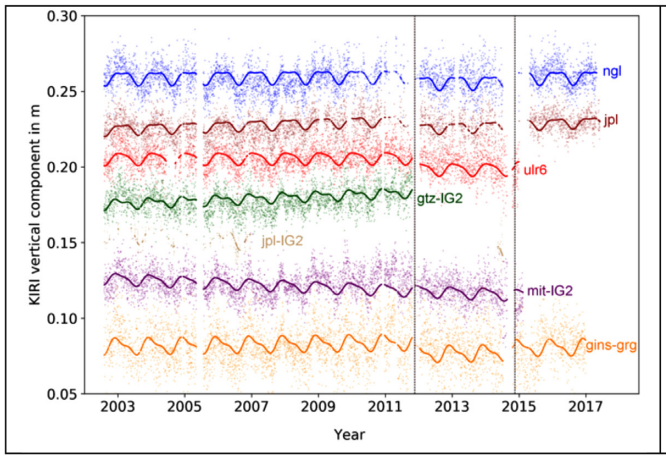

	Common jump				Individual jumps estimates			
	Jump 1	Jump 2	trend	sd	Jump 1	Jump 2	trend	sd
ngl			0,62	0,08	0,1	0,4	-0,2	0,14
jpl			0,88	0,09	-0,3	-0,02	0,7	0,14
ulr6			0,15	0,09	-0,7	-0,9	0,4	0,13
gtz-IG2	-0,5	0,006	0,7	0,12			0,7	0,12
jpl-IG2			-0,14	0,36	1,6		-2,1	1
mit-IG2			-0,07	0,09	-0,7	-1,2	0,21	0,12
gins-grg			0,42	0,09	-0,6	0,05	0,51	0,13
weighted mean on trend :			**0,37**	0,4			**0,03**	0,9

Figure 5. Illuustration of the correlation effect between offset amplitude and estimated trend in the time-series. For this test, we imposed the same discontinuity epochs in all the cases. We, then, tested the impact of modelling a common amplitude discontinuity offset on all the series, or modelling a discontinuity offset specific to each series. In all the test cases, trends were modelled individually, per time-series. The time-series data are shown as pale colour and the model fit for each solution is superimposed in stronger colour. In the KIRI station, the discontinuities are related to material changes. In the case of individual estimates, the table in the right-hand panel illustrates the direct correlation between discontinuity amplitude and associated trend.

of freedom. This approach would be very subjective, as there are no rules for such decimation.

As an alternative way to derive a reasonable uncertainty, we ran a joint inversion with a specific configuration, that is using the same parameters for all the time-series, except for the linear trends which are estimated independently for each time-series. This provides us with an estimate of the uncertainty on the displacement rate from the spread of the individual trends, which accounts for the uncertainty related to the data processing. We finally obtain the total uncertainty of the displacement rates within the ITRF2008 reference frame (σ_{GPS} in Table 3) as the square root of the sum of the variance related to the data processing (spread of trends) and the variance associated with the formal error (output from the least-squares inversion), which represents the misfit.

The second contribution, due to the uncertainty on the ITRF2008 reference frame, cannot be assessed from our GNSS data study itself and needs external information; Altamimi *et al.* (2017) evaluate the difference between ITRF2008 and ITRF2014 to be 0.2 mm yr^{-1} on the scale factor and -0.1 mm yr^{-1} on the Z-axis (the latter term's contribution to the vertical velocity of each station is a function of the sine of the station latitude, reaching a maximum of -0.07 mm yr^{-1} for the southernmost station of our region, CHAT/CHTI on Chatham Island). Based on external evaluations, Collilieux *et al.* (2014) propose that the level of accuracy for ITRF2008 is in the order of 0.5 mm yr^{-1} on each origin component ($\sigma_{origin_{RF}} = 0.5$ mm yr^{-1}) and better than 0.3 mm yr^{-1} on the scale rate ($\sigma_{scale_{RF}} = 0.3$ mm yr^{-1}).

Assuming that the components of the uncertainty are all independent, the final uncertainty (σ_{final}) can be expressed as the quadratic sum of the three components (eq. 3).

$$\sigma_{final} = \sqrt{\sigma^2_{GPS} + \sigma^2_{origin_{RF}} + \sigma^2_{scale_{RF}}}. \quad (3)$$

Table 3. Linear trend of vertical land motion, associated with uncertainties. We provide the uncertainty related to the GNSS data processing, within the working ITRF2008 reference frame, as well as a final uncertainty which accounts also for the uncertainty on the reference frame origin (0.5 mm yr^{-1}) and scale (0.3 mm yr^{-1}). Units: mm yr^{-1}.

Station	Longitude	Latitude	Trend	σ GPS	σ final
ASPA	189.278	−14.326	−0.47	0.68	0.90
AUCK	174.834	−36.603	−0.59	0.22	0.62
CHAT	183.434	−43.956	−0.77	0.22	0.62
CHTI	183.383	−43.735	−1.19	0.86	1.13
CKIS	200.199	−21.201	0.09	0.26	0.64
FALE	188.000	−13.832	−1.74	0.24	0.63
FTNA	181.879	−14.309	−0.47	0.64	0.90
GAMB	225.035	−23.130	−1.33	0.24	0.63
HGHN	164.943	−20.689	−1.33	0.19	0.62
KIRI	172.923	1.355	0.44	0.47	0.69
KOUC	164.287	−20.559	−0.92	0.21	0.62
LAE1	146.993	−6.674	−5.42	0.28	0.65
LAUT	177.447	−17.609	−0.07	0.22	0.62
LDHI	159.079	−31.541	−0.89	0.61	0.84
LORD	159.061	−31.520	−1.04	0.32	0.67
LPIL	167.264	−20.918	−0.67	0.29	0.66
MAJU	171.365	7.119	−1.00	0.52	0.75
NAUR	166.926	−0.552	−0.43	0.67	0.90
NORF	167.939	−29.043	−0.68	0.45	0.74
NOUM	166.410	−22.270	−1.32	0.33	0.67
NRMD	166.485	−22.228	−1.33	0.28	0.64
PAPE	210.427	−17.533	−1.67	0.25	0.63
PNGM	147.366	−2.043	−2.18	0.40	0.71
POHN	158.210	6.960	1.57	0.36	0.69
SAMO	188.262	−13.849	−0.58	0.34	0.67
SOLO	159.954	−9.435	−3.27	0.94	1.11
TAH1	210.394	−17.577	−0.86	0.38	0.82
TAH2	210.394	−17.577	−1.39	0.55	0.80
TBTG	210.524	−23.342	−1.16	0.54	0.76
THIO	166.215	−21.609	−2.02	0.43	0.73
THTI	210.394	−17.577	−0.28	0.16	0.60
TONG	184.821	−21.145	1.57	0.30	0.67
TOW2	147.056	−19.269	−0.58	0.33	0.67
TUVA	179.197	−8.525	−0.80	0.20	0.62
VANU	168.315	−17.744	−4.98	0.28	0.65

Table 4. Excerpt of discontinuities used for the time-series modelling (The full version is available with the online version). The format of the file complies with the classical SINEX format used by IGS. The Solution Number (SOLN) is used to distinguish between periods in the presence of discontinuities. The type of discontinuity is P for Position or V for velocity. Last column is a comment on the origin of the discontinuity when available, with 'Rec.' and 'ant.', respectively, for receiver and antenna.

Station code	Solution number	Time period between discontinuities	Discontinuity type	Comment on discont. origin
ASPA A	1	00:000:00000 08:275:00000	P	Rec. & ant. change
ASPA A	2	08:275:00000 09:272:62 231	P	8.1 (LM)
ASPA A	3	09:272:62 231 00:000:00000	P	
ASPA A	1	00:000:00000 09:272:62 231	V	8.1 (LM)
ASPA A	2	09:272:62 231 00:000:00000	V	
AUCK A	1	00:000:00000 99:350:00000	P	Rec. & ant. change
AUCK A	2	99:350:00000 01:301:00000	P	Rec. & ant. change
AUCK A	3	01:301:00000 05:307:00000	P	Antenna change
AUCK A	4	05:307:00000 06:057:00000	P	Rec. & ant. change
AUCK A	5	06:057:00000 00:000:00000	P	
AUCK A	1	00:000:00000 00:000:00000	V	

Note that this final uncertainty may be a pessimistic estimate if one is interested in relative motion between different stations located in the same area, since part of the error may cancel out, in particular the error on the reference frame, which can be spatially coherent.

4 RESULTS

For each station, position time-series and rates are illustrated in Fig. S2. Rates and uncertainties obtained from the different sources and different methods are given in Table S1. Table 3 summarizes

the results obtained using the joint least-squares inversion (modelling), with all available time-series from different solutions (Section 3.2.2), together with the estimated uncertainty based on a combination of the least-squares misfit, the spread of individually determined trends (Section 3.2.3) and the reference frame uncertainty.

The boxplots presented in Fig. 6 show the spread of individual solutions, as well as the proposed combined solution. The vertical displacement linear rates obtained by the joint modelling are displayed on a regional map in Fig. 7.

In our region, the linear component of vertical displacement, estimated using the assumption that the ground moves linearly between step discontinuities (except for seasonal signals and, in few cases, for post-seismic deformation following major earthquakes), varies from -5.0 ± 0.3 mm yr^{-1} at stations LAE1 (Papua New Guinea) and VANU (Vanuatu) to 1.6 ± 0.4 mm yr^{-1} at stations POHN (Federated States of Micronesia) and TONG (Tonga). The average vertical displacement rate in the area is -1.1 mm yr^{-1}, with a standard deviation of 1.4 mm yr^{-1}; the individual rates are determined with an average uncertainty of 0.4 mm yr^{-1}.

In some cases, modelling the observations with a linear trend (see eq. 1) may not be the most suitable description of the motion: it provides an approximation to be used with caution. This is obviously the case when the station is affected by earthquakes, post-seismic deformation or transient deformation such as slow earthquakes as evidenced in several active tectonic areas (Dragert *et al.* 2001). However, linear rates are commonly used since they often have the advantage of providing a simple and informative first order trend.

5 DISCUSSION

The dominant trend for the linear part of vertical motion in the Southwest and Central Pacific is moderate subsidence, on the order of a millimetre per year (Fig. 7). However, a great variability of type of motion is observed. The first obvious distinction that one should make is based on the presence or absence of earthquake-induced motion in the position time-series. Fig. 3 showed the areas prone to earthquake induced motion and our findings are in agreement with these anticipated areas of motion. Earthquake induced motion can take the form of step discontinuities in the time-series or, for major earthquakes, a change of displacement rate which is reasonably well modelled by a logarithmic and exponential decay in our four case studies. Note that, for ASPA station, the post-seismic fit is degrading in the most recent years (this is seen on the NGL solution which has more recent data) because the hundred-day post-seismic time constant appears to be too short. Another notable feature in our data set is that in the four time-series where post-seismic deformation is visible, it contributes very substantially to the total displacement. This is especially true for the three stations in the Samoa and American Samoa (ASPA, FALE and SAMO) affected by the September 2009 M8.1 Samoa earthquake, for which the coseismic jump is in fact negligible with respect to the post-seismic deformation. Post-seismic deformation, in particular the viscoelastic component, is a large scale and deep origin process which may impact vertical displacement rates in an area much larger than the area affected by coseismic displacement; therefore, stations that are not located in the expected area of motion illustrated in Fig. 3 may still be impacted by tectonic origin processes. This fact should be kept in mind when looking at sites such as MAJU (in the Marshall Islands) or POHN, which are not located in the direct vicinity of tectonic features, such as a plate boundary, but are not very far either from major events such as the March 2011 *M*9 Tohoku earthquake. A discontinuity step is present in the IGS discontinuity table for MAJU station and in the SONEL discontinuity table for both POHN and MAJU stations, which are respectively around 3600 and 4500 km distant from the Tohoku earthquake hypocentre. By contrast, no discontinuity step is estimated for GUAM station, neither in IGS nor SONEL, although the distance to the hypocentre is about 2700 km. These cases illustrate the difficulty in setting step discontinuities in position time-series, together with the fact that estimating a single velocity across the entire data span can be questionable in case of major events such as mega-earthquakes which may modify the long-term velocities of a broad region.

The MIDAS software (Blewitt *et al.* 2016) designed to overcome the difficulty in objectively detecting step discontinuities, has proven its usefulness and efficiency as a trend estimator for GNSS time-series. However, based on the discrepancy between MIDAS and other estimates on a number of stations (disregarding the stations with a post-seismic signal, for which the functional models are not identical), we find that MIDAS' automatic procedure may be sometimes hazardous for the vertical component, especially for local scale studies requiring mm yr^{-1} level accuracy. It is the case in particular for stations with a strong post-seismic signal, such as SAMO, since MIDAS is a trend estimator and is not designed to account for logarithmic or exponential type of signals. It is also the case for other stations, such as SOLO, TONG or NRMD, for which the number of discontinuities estimated automatically by MIDAS (see last column in file http://geodesy.unr.edu/velocities/midas.IGS08.txt) is much higher than those identified manually and corresponding to material changes or significant earthquakes.

NRMD Noumea station, located in New Caledonia, is another interesting situation (Fig. 2). A recent study combining satellite altimetry and tide gauge data suggests that the tide gauge is uplifting (Aucan *et al.* 2017). This is in contrast with most geodetic estimates which indicates a subsidence for this station (see Table S1). However, the NGL-Midas solution and the JPL-Nasa solution both indicate uplift at NRMD. The linear trend estimate for NRMD is highly sensitive to the input (or not) of a step discontinuity in 2009, when the GNSS equipment (antenna and receiver) was changed. The IGS and SONEL discontinuity tables include a discontinuity for this equipment change, whereas the JPL discontinuity table does not. Reprocessing the JPL and NGL position time-series with our discontinuity table (and thus a discontinuity in 2009 for NRMD) leads to a negative trend, indicating subsidence (Fig. 2). This case further illustrates the crucial impact of the step discontinuity choice, especially when discontinuities are located near the middle of the time-series. In the Noumea case, the question is still opened and assessing the linear trend of vertical motion is delicate.

Only two stations, POHN and TONG, respectively, located in Pohnpei in the Federated States of Micronesia and Nuku'Alofa in Tonga, seem to be uplifting (1.6 ± 0.4 mm yr^{-1} for POHN, 1.6 ± 0.3 mm yr^{-1} for TONG). Our solution also shows a possible uplift (0.4 ± 0.4 mm yr^{-1}) for KIRI station. All other stations do not move significantly (CKIS) or are subsiding (negative trends). The functional model contains several terms, including the trend and step discontinuities, which can play in opposite directions but, overall, even when accounting for earthquake induced step discontinuities in the integrated vertical land movement, most stations are experiencing subsidence. The notable exceptions are the three above-mentioned stations (POHN, TONG and KIRI) for which the linear trend estimate is positive and VANU station, which is experiencing a net uplift despite a clear linear subsidence (-5.0 ± 0.3 mm yr^{-1})

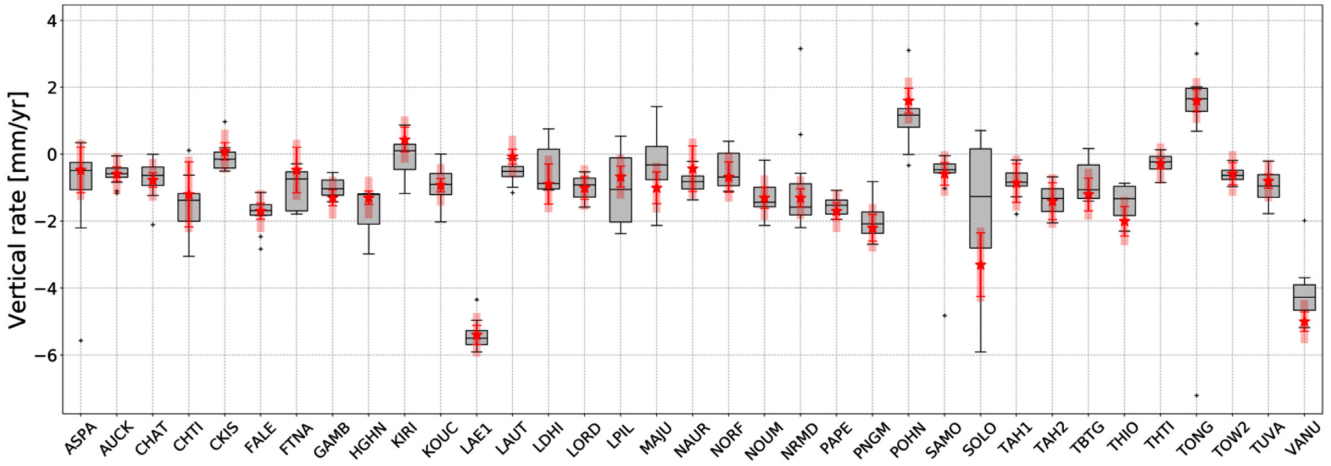

Figure 6. Boxplot diagram showing the spread of vertical displacement rates, for each station, from the different analysis centres and the proposed solution (in red). The range of solutions for each station is displayed using classical boxplots. The box limits correspond to the first quartile (Q1, 25th percentile) and third quartile (Q3, 75th percentile) of the data distribution, and the horizontal line in the box corresponds to the median value. The black error bars indicate the minimum and maximum values, defined for boxplots respectively as Q1–1.5∗IQR and Q3 + 1.5∗IQR, IQR being the interquartile range (Q3–Q1). Outliers are represented by crosses outside the box. The red star indicates the joint solution obtained in our study; the red error bar corresponds to the standard deviation σ_{GPS} associated with the GPS rate estimate within the ITRF2008 reference frame. The light red large bar indicates the proposed final uncertainty estimate which also includes the uncertainty due to the reference frame definition and stability.

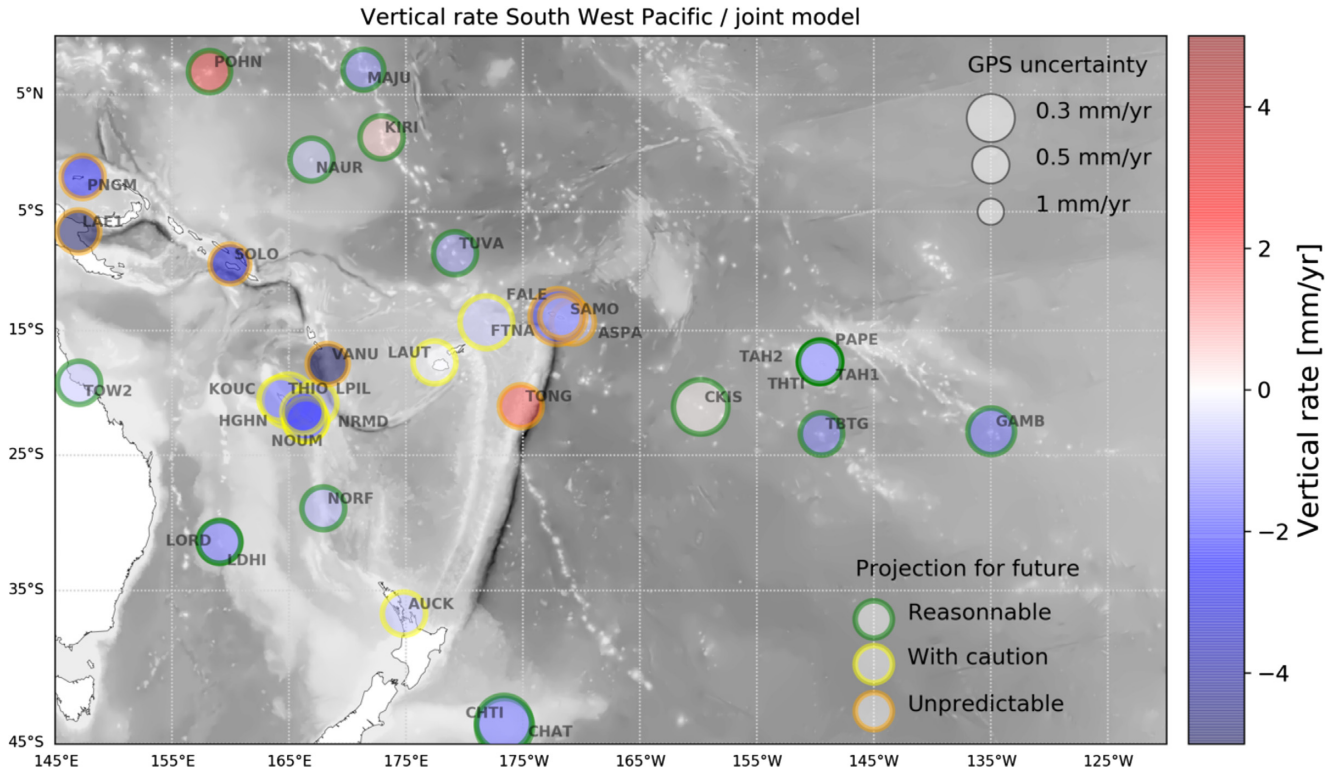

Figure 7. Vertical land motion from available GNSS in the Southwest and Central Pacific and associated predictability. The background grey shading highlights the bathymetric features in the oceanic domain, based on GEBCO_2014 data (Weatherall *et al.* 2015). The displayed vertical displacement values are the values obtained by a joint inversion of the available time-series (see text for details) using a single set of discontinuities, with commonly estimated jumps amplitudes, trends and post-seismic deformation (when needed). The uncertainty is displayed on the map by the size of the circles, inversely proportional to the uncertainty values (most resolved values are shown by large circles, to increase their visibility); the uncertainty used here corresponds to the uncertainty of the GPS computation itself (σ_{GPS} in Table 3). The 'projection for future' criteria, based on the geodynamic context for each station, is given by the colour of each circle contour.

before a sequence of earthquakes whose uplift dominates the vertical displacement behaviour. This latter case is illustrative of the difficult task of accounting for vertical land motion at tide gauge location for instance for sea level studies.

Another notable case study is that of Papeete in the French Polynesia, where four GNSS stations are located within 7 km from each other (PAPE, TAH1, TAH2, THTI), with PAPE located at the tide gauge, whereas TAH1,TAH2 and THTI are inland, more than 80 m above mean sea level at the University facility. PAPE suggests coastal subsidence in contrast with the stability indicated by THTI. This case study may be an illustration of the point-wise information provided by GNSS stations, already noted in previous studies and other Earth surface processes (e.g. Raucoules *et al.* 2013). The large uncertainties on the rates estimated from TAH1 and TAH2 and the difference with the nearby site of THTI also illustrates the possible contribution of error sources other than data processing (e.g. monumentation or equipment). Finally, this case highlights the necessary caution required when spatially extrapolating GNSS estimates of vertical land motion, even at a few kilometres distance.

To conclude this discussion, we address the general question that non-specialists may have about the impact of vertical land motion in future sea levels at the coast, using a few demonstrative cases. Besides obtaining the best estimate of linear trends from multiple high-precision GNSS solutions, one of the objectives of our study was to evaluate the contribution of vertical land motion to relative sea level, and to assess whether or not this contribution can be forecast for future relative sea levels. One relevant question for the adaptation to future sea level rise and coastal management planning is the following: is the fairly steady behaviour of a position time-series and the absence of significant earthquake-induced discontinuities over several years or even decades a sufficient criterion for extrapolation into the future? The position time-series of LAE1, located in Lae in Papua New Guinea, illustrates this point: the station position motion appears nearly linear since the installation of the GNSS station in 2001, but the station is located in a highly seismic area, so one can reasonably expect that significant and sudden vertical displacements will occur in the near future. The current strong subsidence (Table 3) is likely to be the surface expression of strain accumulation on a subsurface fault and it is not reasonable to use the current rates of vertical land motion in LAE1 for long-term projection of relative sea level. The coloured circles on Fig. 7 show the level of confidence we propose for extrapolating current vertical displacement rates into the future.

The last part of our discussion concerns the suitability of the GINS software for the study of long-term slow Earth surface movements. Our results show that the GINS solutions of vertical displacement rates are consistent with the results published by other groups. Although the performance of the GINS solutions are probably not yet at the level of the best available solutions, the ease of implementation makes it a good alternative option for many geophysical studies when the data span is long enough.

6 CONCLUDING REMARKS

This study addresses how to deal with and/or choose between the multiple high-precision GNSS solutions easily and freely available from various renowned analysis centres, and explains the significant differences in the estimates of vertical land motion that can be observed from one solution to the other at a number of stations in a given region. The Southwest and Central Pacific was chosen as a case study because of the clear differences in solutions and the high stakes of using the 'right' solution; however, our approach can be transposed to other regions. We show that significant differences remain even after taking into account the methodological differences in the inversion procedures to estimate GNSS velocities from the daily position time-series of the various groups. The question then is: how to choose among the available GNSS solutions? Instead of choosing at random or subjectively, we propose a least squares inversion using a joint model that considers all the available position time-series and that provides reasonable uncertainties taking into account the noise content in the time-series but also the differences in the data processing between the GNSS solutions and the reference frame uncertainty.

We applied the method in the Southwest and Central Pacific and obtained a new set of vertical velocity at GNSS stations with reasonable uncertainties for further geophysical interpretation. In this region, the order of magnitude of vertical displacement rates is often close to the order of magnitude of sea level rise; anticipating the evolution of future sea level rise relative to the coast, in particular for the development of adaptation strategies, requires an assessment not only of the current value of vertical displacement rates, but also of its future predictability. We have combined the results on current land motion with information on the geodynamic context to propose both linear rates, associated uncertainties and predictability criteria (Fig. 7).

We illustrated that, even using careful data processing and methodology, the sometimes-arbitrary choice of including a step discontinuity at a specific epoch can be critical in the final trend estimate of vertical displacement. One direct implication of this observation is that equipment changes must be minimized when targeting high accuracy positioning. Our approach also demonstrates the interest of having multiple analysis centres processing the data for each station, as different and reasonable assumptions can provide different results, which should be a red flag to the user against using any one solution, without knowing the assumptions behind individual solution.

ACKNOWLEDGEMENTS

This work was supported by CNES through the TOSCA program and the French research agency (Agence Nationale de la Recherche; ANR) under the STORISK project (NR-15-CE03-0003). The IGS, NGL, JPL/NASA and SONEL services are acknowledged for providing access to GNSS time-series and data, which are available thanks to the institutions which contribute their observations freely to these scientific services. We thank Geoscience Australia, which is a major data provider in the Pacific, in the framework of the former South Pacific Sea Level and Climate Monitoring Project, now continued as Pacific Sea Level Monitoring Project under the Climate and Oceans Support Program in the Pacific (http://www.bom.gov.au/pacific/projects/pslm/). We thank the CNES for providing the GINS software used to generate GPS time-series, F. Perosanz, J. Marty and S. Loyer for their help on the use of GINS software and M. Bos for providing the HECTOR software used to analyse the GPS time-series within this study. We benefited from the Global CMT project and used their earthquake catalogue. We thank P. Valty for discussions on GNSS data processing in the Pacific. Finally, we thank the editor, D. Agnew, and the two reviewers, S. Williams and D. Argus, for their comments and help to improve the manuscript.

REFERENCES

Ablain, M. *et al.*, 2015. Improved sea level record over the satellite altimetry era (1993–2010) from the Climate Change Initiative project, *Ocean Sci.,* **11,** 67–82.

Altamimi, Z., Boucher, C. & Sillard, P., 2002. New trends for the realization of the International Terrestrial Reference System, *Adv. Sp. Res.,* **30,** 175–184.

Altamimi, Z., Collilieux, X., Legrand, J., Garayt, B. & Boucher, C., 2007. ITRF2005: a new release of the International Terrestrial Reference Frame based on time series of station positions and Earth Orientation Parameters, *J. geophys. Res.: Solid Earth,* **112,** 1–19.

Altamimi, Z., Métivier, L., Rebischung, P., Rouby, H. & Collilieux, X., 2017. ITRF2014 plate motion model, *Geophys. J. Int.,* **209,** 1906–1912.

Argus, D.F., Peltier, W.R., Drummond, R. & Moore, A.W., 2014. The Antarctica component of postglacial rebound model ICE-6G_C (VM5a) based on GPS positioning, exposure age dating of ice thicknesses, and relative sea level histories, *Geophys. J. Int.,* **198,** 537–563.

Aucan, J., Merrifield, M.A. & Pouvreau, N., 2017. Historical Sea Level in the South Pacific from Rescued Archives, Geodetic Measurements, and Satellite Altimetry, *Pure appl. Geophys.,* **174,** 3813–3823.

Becker, M., Meyssignac, B., Letetrel, C., Llovel, W., Cazenave, A. & Delcroix, T., 2012. Sea level variations at tropical Pacific islands since 1950, *Glob. Planet. Change,* **80–81,** 85–98.

Bevis, M. & Brown, A., 2014. Trajectory models and reference frames for crustal motion geodesy, *J. Geod.,* **88,** 283–311.

Blewitt, G., Kreemer, C., Hammond, W.C. & Gazeaux, J., 2016. MIDAS robust trend estimator for accurate GPS station velocities without step detection, *J. geophys. Res.: Solid Earth,* **121,** 2054–2068.

Blewitt, G. & Lavallée, D., 2002. Effect of annual signals on geodetic velocity, *J. geophys. Res.,* **107,** 2145.

Bos, M.S., Fernandes, R.M.S., Williams, S.D.P. & Bastos, L., 2013. Fast error analysis of continuous GNSS observations with missing data, *J. Geod.,* **87,** 351–360.

Collilieux, X. *et al.*, 2014. External evaluation of the terrestrial reference frame: report of the task force of the IAG sub-commission 1.2, in *Earth Edge Sci. a Sustain. Planet,* Vol. **139,** pp. 197–202, eds Rizos, C. & Willis, P., Springer Berlin Heidelberg.

Collilieux, X., Métivier, L., Altamimi, Z., Dam, T. van & Ray, J., 2011. Quality assessment of GPS reprocessed terrestrial reference frame, *GPS Solut.,* **15,** 219–231.

Collilieux, X. & Wöppelmann, G., 2011. Global sea-level rise and its relation to the terrestrial reference frame, *J. Geod.,* **85,** 9–22.

Darwin, C., 1842. *The Structure and Distribution of Coral Reefs: Being the First Part of the Geology of the Voyage of the Beagle, Under the Command of Capt. Fitzroy, R.N. During the Years 1832 to 1836,* Geology Of The Voyage Of The Beagle, Smith, Elder and Company. Retrieved from https://books.google.fr/books?id=qLsQAAAAIAAJ.

DeMets, C., Gordon, R.G. & Argus, D.F., 2010. Geologically current plate motions, *Geophys. J. Int.,* **182,** 1–80.

Dow, J.M., Neilan, R.E. & Rizos, C., 2009. The International GNSS Service in a changing landscape of Global Navigation Satellite Systems, *J. Geod.,* **83,** 191–198.

Dragert, H., Kelin, W. & James, T.S., 2001. A silent slip event on the deeper Cascadia subduction, *Science (80-).,* **292,** 1525–1528.

Fund, F., Perosanz, F., Testut, L. & Loyer, S., 2013. An integer precise point positioning technique for sea surface observations using a GPS buoy, *Adv. Sp. Res.,* **51,** 1311–1322.

Gazeaux, J. *et al.*, 2013. Detecting offsets in GPS time series: first results from the detection of offsets in GPS experiment, *J. geophys. Res.: Solid Earth,* **118,** 2397–2407.

Griffiths, J. & Ray, J., 2016. Impacts of GNSS position offsets on global frame stability, *Geophys. J. Int.,* **204,** 480–487.

Heflin, 2018. Introduction to JPL's GPS Time Series.

Heflin, M.B. *et al.*, 1992. Global geodesy using GPS without fiducial sites, *Geophys. Res. Lett.,* **19,** 131–134.

Lagler, K., Schindelegger, M., Böhm, J., Krásná, H. & Nilsson, T., 2013. GPT2: empirical slant delay model for radio space geodetic techniques, *Geophys. Res. Lett.,* **40,** 1069–1073.

Langbein, J., 2012. Estimating rate uncertainty with maximum likelihood: differences between power-law and flicker-random-walk models, *J. Geod.,* **86,** 775–783.

Legrand, J., Bergeot, N., Bruyninx, C., Wöppelmann, G., Bouin, M.-N. & Altamimi, Z., 2010. Impact of regional reference frame definition on geodynamic interpretations, *J. Geodyn.,* **49,** 116–122.

Mao, A., Harisson, C.G.A.A. & Dixon, T.H., 1999. Noise in GPS coordinate time series, *J. geophys. Res.: Solid Earth,* **104,** 2797–2816.

Martínez-asensio, A., Wöppelmann, G., Ballu, V., Becker, M., Testut, L. & Magnan, A.K., 2019. Relative sea-level rise and the in fl uence of vertical land motion at Tropical Pacific Islands, *Glob. Planet. Change,* **176,** 132–143.

Marty, J.C. *et al.*, 2011. GINS: the CNES/GRGS GNSS scientific software, in *ESA Proceedings WPP326 3rd Int. Colloq. Sci. Fundam. Asp. Galileo Program*.

Métivier, L., Collilieux, X., Lercier, D., Altamimi, Z. & Beauducel, F., 2014. Global coseismic deformations, GNSS time series analysis, and earthquake scaling laws, *J. geophys. Res.: Solid Earth,* **119,** 9095–9109.

Nurse, L.A., McLean, R.F., Agard, J., Briguglio, L.P., Duvat-Magnan, V., Pelesikoti, N., Tompkins, E. & Webb, A., 2014. Small islands, in *Climate Change 2014: Impacts, Adaptation, and Vulnerability. Part B: Regional Aspects. Contribution of Working Group II to the Fifth Assessment Report of the Intergovernmental Panel of Climate Change,* pp. 1613–1654, eds Barros, V.R., *et al*., Cambridge University Press.

Okada, Y., 1985. Surface deformation due to shear and tensile faults in a half-space, *Bull. seism. Soc. Am.,* **75,** 1135. Retrieved from http://dx.doi.org/.

Pelletier, B., Calmant, S. & Pillet, R., 1998. Current tectonics of the Tonga-New Hebrides region, *Earth planet. Sci. Lett.,* **164,** 263–276. Retrieved from file:////Users/vballu/References/Pdfs_Javier/Pelletier1998.pdf.

Peltier, W.R., Argus, D.F. & Drummond, R., 2015. Space geodesy constrains ice age terminal deglaciation: the global ICE-6G_C (VM5a) model, *J. geophys. Res.: Solid Earth,* **120,** 450–487.

Petit, G. & Luzum, B., 2010. IERS Conventions (2010), IERS Tech. Note, 36.

Pirazzoli, P. & Montaggioni, L., 1985. Lithosphere deformation in French Polynesia (French Pacific) as deduced from Quaternary shorelines, in *Proceedings of the 5th Int. Coral Reef Congr.,* Vol. **3,** pp. 195–200, Tahiti.

Raucoules, D., Cozannet, G. Le, Wöppelmann, G., Michele, M. de, Gravelle, M., Daag, A. & Marcos, M., 2013. High nonlinear urban ground motion in Manila (Philippines) from 1993 to 2010 observed by DInSAR: implications for sea-level measurement, *Remote Sens. Environ.,* **139,** 386–397.

Rebischung, P., Altamimi, Z., Ray, J. & Garayt, B., 2016. The IGS contribution to ITRF 2014, *J. Geod.,* **90,** 611–630.

Rebischung, P., Ray, J., Benoist, C., Métivier, L. & Altamimi, Z., 2015. Error analysis of the IGS repro2 station position time series, *Am. Geophys. Un., Fall Meet. 2015,* abstract G23B–1065.

Santamaría-Gómez, A., Bouin, M.-N., Collilieux, X. & Wöppelmann, G., 2011. Correlated errors in GPS position time series: Implications for velocity estimates, *J. geophys. Res.: Solid Earth,* **116,** 1–14.

Santamaría-Gómez, A., Gravelle, M., Dangendorf, S., Marcos, M., Spada, G. & Wöppelmann, G., 2017. Uncertainty of the 20th century sea-level rise due to vertical land motion errors, *Earth planet. Sci. Lett.,* **473,** 24–32.

Stammer, D., Cazenave, A., Ponte, R.M. & Tamisiea, M.E., 2013. Causes for contemporary regional sea level changes, *Ann. Rev. Mar. Sci.,* **5,** 21–46.

Steigenberger, P., Rothacher, M., Dietrich, R., Fritsche, M., Rülke, A. & Vey, S., 2006. Reprocessing of a global GPS network, *J. geophys. Res.: Solid Earth,* **111,** doi:10.1029/2005JB003747.

Wang, W., Zhao, B., Wang, Q. & Yang, S., 2012. Noise analysis of continuous GPS coordinate time series for CMONOC, *Adv. Sp. Res.,* **49,** 943–956, COSPAR.

Weatherall, P. *et al.*, 2015. A new digital bathymetric model of the world's oceans, *Earth Sp. Sci.,* 1–15, doi:10.1002/2015EA000107.

Williams, S.D.P., 2003. Offsets in Global Positioning System time series, *J. geophys. Res.: Solid Earth,* **108,** doi:10.1029/2002JB002156.

Williams, S.D.P., 2008. CATS: GPS coordinate time series analysis software, *GPS Solut.,* **12,** 147–153.

Williams, S.D.P., Bock, Y., Fang, P., Jamason, P., Nikolaidis, R.M., Prawirodirdjo, L., Miller, M. & Johnson, D.J., 2004. Error analysis of continuous GPS position time series, *J. geophys. Res.,* **109,** B03412.

Wöppelmann, G. & Marcos, M., 2016. Vertical land motion as a key to understanding sea level change and variability, *Rev. Geophys.,* **54,** 64–92.

Wöppelmann, G., Martin Miguez, B., Bouin, M.-N. & Altamimi, Z., 2007. Geocentric sea-level trend estimates from GPS analyses at relevant tide gauges world-wide, *Glob. Planet. Change,* **57,** 396–406.

Wyett, K., 2014. Escaping a Rising Tide: Sea Level Rise and Migration in Kiribati, *Asia Pacific Policy Stud.,* **1,** 171–185.

SUPPORTING INFORMATION

Supplementary data are available at *GJI* online.

Table S1. Vertical rates and associated standard deviations extracted from available databases (for centres labelled ngl-Midas, jpl-Nasa and ulr6-Sonel), or estimated from available time-series (all the other centres). Rates and standard deviations for centres labelled IG2 are estimated from coordinate time-series made available by processing centres as part of the IGS REPRO2 reprocessing campaign. IG2c indicates trend estimates done using CATREF combination and alignment software (Altamimi *et al.*, Rebischung *et al.*) combinaing all the stations in the same minimization, others are obtained using Hector software on individual timeseries. Itrf2014 corresponds to the rates and standard deviation values given in the ITRF2014. gins-grg and joint-model correspond, respectively, to the solution obtained using GINS software and the joint modelling proposed in this study.

Table S4. List of discontinuities used for the time-series modelling. These discontinuities were used in the modelling of each time-series analysis using Hector software and in the joint least-squares modelling of all the time-series available for each station. The format of the file is an extract of the classical SINEX format used by IGS. CODE is the 4-digit code of each station, PT refers to the identity of the point in case of multiple points, SOLN corresponds to the Solution Number to distinguish between periods in the presence of discontinuities, T_DATA_START and T_DATA_END are, respectively, the start and end limits of the period, M is the type of discontinuity and can be P for Position or V for velocity and A is a comment on the origin of the discontinuity when available.

Table S5. List of parameters (common slope, β, common amplitude of steps γ_i for the *i*th discontinuity, common amplitude of logarithmic decay, γ, common amplitude of exponential decay, ε) obtained in the joint inversion for each station. Note that the amplitude of the logarithmic and exponential post-seismic parameters have been estimated with an arbitrary relaxation time.

Please note: Oxford University Press is not responsible for the content or functionality of any supporting materials supplied by the authors. Any queries (other than missing material) should be directed to the corresponding author for the paper.